Patchy propagators, brain dynamics, and the generation of spatially structured gamma oscillations

P. A. Robinson
School of Physics, University of Sydney, New South Wales 2006, Australia
and Brain Dynamics Center, Westmead Millenium Institute, Westmead Hospital and Western Clinical School of The University of Sydney, Westmead, New South Wales 2145, Australia
(Received 23 November 2005; published 7 April 2006)

Propagator theory of brain dynamics is generalized to incorporate a new class of patchy propagators that enable treatment of approximately periodic structures such as are seen in the visual cortex. Complex response fields are also incorporated to allow for features such as orientation preference and wave-number selectivity. The results are applied to the corticothalamic system associated with the primary visual cortex. It is found that this system can generate gamma ($\gtrsim$30 Hz) oscillations during stimulation, whose properties are consistent with experimental findings on gamma frequency and bandwidth, and existence of fine-scale spatial structure. It is found that a potential resonance is associated with each reciprocal lattice vector corresponding to periodic modulations of the propagators. It is found that the lowest resonances are the most likely to give rise to noticeable spectral peaks and increases of correlation amplitude, length, and time, and that these aspects are prominent only if the system is close to marginal stability, in accord with previous measurements and discussions of cortical stability. These features also enable gamma resonances to be stimulus-evoked, with substantial resonance sharpening for relatively small changes in mean neural firing rate. The results also imply dependence of gamma frequency on stimulus features.

DOI: 10.1103/PhysRevE.73.041904 PACS number(s): 87.10.+e, 87.19.La, 87.19.Nn

I. INTRODUCTION

Recent work on physiologically based continuum modeling of brain dynamics has resulted in numerous quantitatively verified predictions of brain electrical activity, including electroencephalogram (EEG) time series, spectra, coherence, and correlations, evoked response potentials, and seizure dynamics. Inversion of the model projections has also yielded estimates of underlying physiological parameters and their variations across the brain, in different states of arousal, and disorders. Overviews of the development of this field exist [1–3], so these are not repeated here.

It has been shown recently that the inclusion of more realistic propagators can yield enhancements of gamma ($>$30 Hz) activity for some parameters, and that this has a broad, relatively structureless wave-number spectrum, extending to high wave numbers [2]. However, it was argued that the spatiotemporal properties of the oscillations found in this previous work did not accord with the fine spatial structure of correlations seen in the visual cortex during perceptual tasks, for example [4–19]. It was suggested that the approximately periodic structure of the visual cortex may lead to finer-scale structure in the gamma response of the visual system that would accord with observations. These observations are of central interest to a wide range of studies of visual response and perception, since they appear to be closely associated with (i.e., either facilitating or reflecting) the binding of disparate features into unified percepts—a critical high-level stage in perception.

It has been shown that the intracortical connections in primary visual cortex are patchy on a scale of millimeters, with preferential connections between regions of like feature preference [4,10,20,21], and this aspect of approximate periodicity was speculated to be the specific mechanism for inducing spatial structure in gamma oscillations [2,8], and has also been considered in connection with hallucinations [21,22]. This paper explores this suggestion quantitatively.

In Sec. II we briefly outline our previous theory. In Sec. III it is generalized to allow for cells with more general receptive fields than have previously been included. In Sec. IV it is further generalized to include patchy propagators, based on physiological and anatomical insights. In Sec. V linear properties are derived and, in Sec. VI, we apply the results to study gamma resonances by generalizing our widely successful corticothalamic model to incorporate the more general propagators.

II. EXISTING THEORY

As in previous work we make a continuum approximation in which neural properties are averaged over linear scales of a tenth of a mm or so: sufficient to contain large numbers of neurons, but small enough to resolve fine structures in the brain.

We assume that the brain contains multiple populations of neurons, distinguished by a subscript a, which simultaneously labels both the structure in which a given population lies (e.g., a particular nucleus) and the type of neuron (e.g., interneuron, pyramidal cell). The continuum soma potential V_a is the sum of contributions V_{ab} arriving as a result of activity at each type of (mainly) dendritic synapse b; b denotes both the population and neurotransmitter type. Thus we write

$$V_a(\mathbf{r},t) = \sum_b V_{ab}(\mathbf{r},t), \tag{1}$$

where $\mathbf{r}$ denotes the spatial coordinates, t the time, the summation is assumed to be linear, and all potentials are mea-

sured relative to resting. The cortex is approximated as a two-dimensional sheet and $\mathbf{r}$ is assumed to be the actual position in the case of the cortex; many other structures, such as the thalamus, are linked to the cortex via a primary topographic map that links points in a one-to-one manner between structures, so we assign the same value of $\mathbf{r}$ to such points. Hence, in structures other than the cortex, the map coordinate $\mathbf{r}$ denotes a *rescaled* physical dimension (i.e., the physical coordinate multiplied by the ratio of the cortical scale to the structure's scale), a point that must be remembered when considering values of spatial parameters in these structures.

The subpotentials V_{ab} respond in different ways to incoming spikes, depending on their synaptic dynamics (ion-channel kinetics, diffusion in the synaptic cleft, etc.), and on subsequent signal dispersion in the dendrites. The resulting soma response to a delta-function input at the synapse can be approximated via the differential equation [23]

$$D_{ab}(\mathbf{r},t)V_{ab}(\mathbf{r},t) = P_{ab}(\mathbf{r},t), \tag{2}$$

$$D_{ab}(\mathbf{r},t) = \frac{1}{\alpha_{ab}(\mathbf{r},t)\beta_{ab}(\mathbf{r},t)}\frac{d^2}{dt^2} + \left[\frac{1}{\alpha_{ab}(\mathbf{r},t)} + \frac{1}{\beta_{ab}(\mathbf{r},t)}\right]\frac{d}{dt} + 1, \tag{3}$$

where P_{ab} is a weighted average number of incoming spikes arriving at $\mathbf{r}$ and t. The parameter α_{ab} is the mean decay rate of the soma response to a delta-function synaptic input, while β_{ab} is the mean rise rate.

In cells with voltage-gated ion channels, action potentials are produced at the axonal hillock when the soma potential exceeds a threshold θ_a. When averaged over a population of neurons with normal response characteristics, a good approximation to the firing rate Q_a is

$$Q_a(\mathbf{r},t) = Q_{a\,\max}S_a[V_a(\mathbf{r},t)], \tag{4}$$

where $Q_{a\,\max}$ is the maximum firing rate and S_a is commonly approximated as

$$S_a[V_a(\mathbf{r},t)] = \frac{1}{1+\exp[-\{V_a(\mathbf{r},t)-\theta_a(\mathbf{r},t)\}/\tilde{\sigma}_a(\mathbf{r},t)]}, \tag{5}$$

where $\sigma_a = \tilde{\sigma}_a\pi/\sqrt{3}$ is the population standard deviation of the firing threshold θ_a.

Spatiotemporal propagation of pulses within and between populations determines the values of P_{ab} in Eq. (2) based on the values of Q_b at other locations and earlier times. Assuming linear propagation, $P_{ab}(\mathbf{r},t)$ can be approximated in terms of an integral over a propagator Λ_{ab} that incorporates a propagator $\Gamma_{ab}(\mathbf{r},t,\mathbf{r}',t')$ for the effects of source activity $Q_b(\mathbf{r}',t')$ to propagate to $\mathbf{r},t$, including discrete time delays $\tau_{ab}(\mathbf{r},\mathbf{r}'t)$ between remotely situated populations, and couplings $\hat{\nu}_{ab}(\mathbf{r},t)$. The latter are operators that take weighted averages over the dendritic arbor of quantities relating closely to the incoming field, its first and second spatial derivatives, and its first temporal derivative—quantities to which certain cells are known to be sensitive [24,25]. The use of an operator generalizes our previous analyses, which treated ν_{ab} as a purely local scalar; it is essential to incorporate microscopic receptive field properties into continuum modeling, analogous to the use of Eq. (5) to represent a population average firing-rate response. The above steps yield

$$P_{ab}(\mathbf{r},t) = \int \Lambda_{ab}(\mathbf{r},t;\mathbf{r}',t')Q_b(\mathbf{r}',t')d\mathbf{r}'dt' \tag{6}$$

$$= \hat{\nu}_{ab}(\mathbf{r},t)\int \delta[t-t'-\tau_{ab}(\mathbf{r},\mathbf{r}',t)] \times \Gamma_{ab}(\mathbf{r},t;\mathbf{r}',t')Q_b(\mathbf{r}',t')d\mathbf{r}'dt' \tag{7}$$

$$= \hat{\nu}_{ab}(\mathbf{r},t)\phi_{ab}[\mathbf{r},t-\tau_{ab}(\mathbf{r},\mathbf{r}',t)], \tag{8}$$

where comparison of Eqs. (7) and (8) defines the pulse density field ϕ_{ab} that comprises signals from population b to a. Equation (8) encapsulates propagation from soma location to soma location. The effective range r_{ab} of the propagator accounts for the coordinate divergence h_{ab} of fibers traveling from b to a and the extent of arborization d_a of dendritic trees of type a, giving an approximate range $r_{ab}=(h_{ab}^2+d_a^2)^{1/2}$. In the case where ν_{ab} is a local coupling-strength function, it is written

$$\nu_{ab}(\mathbf{r},t) = N_{ab}(\mathbf{r},t)s_{ab}(\mathbf{r},t), \tag{9}$$

where N_{ab} is the mean number of connections from cells of type b per cell of type a and s_{ab} is their mean strength.

The index a includes all populations whose activity can be modified by incoming stimuli. The index b also labels stimulus types (e.g., left and right eye, color, etc., with a separate value of b for each type of stimulus, in general). This separation of stimuli into subtypes is necessary to allow for competition in development and learning, for example, but can be dispensed within applications where this distinction is not relevant.

Considerable work has shown that, to a good approximation, signals propagate within a smoothly structured neural population as if governed by a damped wave equation and, hence, that a wave propagator can be used [2,23]. This has the major advantage of enabling the propagation of ϕ_{ab} to be treated in differential form, rather than via the integral equation (6) or (7).

For an isotropic damped wave equation of the form

$$\left[\frac{1}{\gamma_{ab}^2}\frac{\partial^2}{\partial t^2} + \frac{2}{\gamma_{ab}}\frac{\partial}{\partial t} + 1 - r_{ab}^2\nabla^2\right]\phi_{ab}(\mathbf{r},t) = Q_b(\mathbf{r},t), \tag{10}$$

$\gamma_{ab}=v_{ab}/r_{ab}$ is the temporal damping coefficient and v_{ab} is the wave velocity in coordinate units. Equation (10) is also satisfied if ϕ_{ab} is replaced by $\Gamma_{ab}^{(0)}(\mathbf{r}-\mathbf{r}',t-t')$ and the right side is replaced by a source of the form $\delta(\mathbf{r}-\mathbf{r}')\delta(t-t')$. This gives

$$\Gamma_{ab}^{(0)}(\mathbf{k},\omega) = \frac{1}{(k^2+q_{0ab}^2)r_{ab}^2}, \tag{11}$$

$$q_{0ab}^2 r_{ab}^2 = (1 - i\omega/\gamma_{ab})^2. \quad (12)$$

The reciprocal of Eq. (11) is the dispersion operator.

III. RECEPTIVE-FIELD COUPLING OPERATORS

The next generalization to our model is to allow for more flexible and realistic forms of the coupling operators that correspond to cellular receptive fields. In the simplest case, the coupling operators $\hat{\nu}_{ab}$ are simply functions that measure the strength of coupling from population b to population a, as in Eq. (9). In a continuum theory, such as the present one, this actually represents a weighted average coupling over a small zone surrounding the point in question, owing to the finite spread of the dendritic arbors of the neurons in this vicinity. In the present analysis we have absorbed the transverse propagation implicit in this spreading into the propagators $\Gamma_{ab}^{(0)}$ via small changes to their effective ranges. However, the spatial averaging introduces low-pass spatial filter characteristics. More generally, the mean receptive-field properties of cells in a given small area can have the effect of performing a spatial average over a kernel function that yields spatially low-pass filtered representations of the derivative, second derivative, and time derivative of the incoming field ϕ_{ab} [24–26]. Some receptive fields appear to act as waveletlike filters, or they approximately perform a locally windowed spatial Fourier sine or cosine transform, for example [26]. The receptive-field coupling operators are integrodifferential operators in general.

In a continuum theory, the effects of the coupling operators must be represented in an averaged sense, rather than including the microscopic properties of individual cells explicitly. This is analogous to replacing the threshold firing behavior of cells by a population representation via the sigmoid function (5). For differential operators O in time and space, we can write

$$\hat{\nu}[O\phi](\mathbf{r},t) = \int d\mathbf{R} \int_{-\infty}^{0} dT [Ow(\mathbf{R},T)]\phi(\mathbf{r}-\mathbf{R},t-T), \quad (13)$$

where we use the result that the Fourier transforms of $[Ow]\phi$ and $w[O\phi]$ are equal to infer that Eq. (13) returns the weighted average of $O\phi$. The kernel w is a function localized on spatial and temporal scales d_a and t_a, respectively. The exact form is not precisely known, nor are results strong functions of this form. In order to obtain simple Fourier properties, we most often use

$$w(\mathbf{k},\omega) = \frac{1}{1 + k^2 d_a^2}, \quad (14)$$

for purely spatial receptive fields, which yields

$$w(\mathbf{R},T) = \frac{1}{2d_a} e^{-|x|/d_a}, \quad (15)$$

$$w(\mathbf{R},T) = \frac{1}{2\pi d_a^2} K_0(R/d_a), \quad (16)$$

in one and two dimensions, respectively, where K_0 is a modified Bessel function of the second kind (a Macdonald function) [27].

IV. PATCHY PROPAGATION

In the present work, we wish to enable treatment of approximately periodic systems, such as are found in the visual cortex (e.g., ocular-dominance columns and orientation-preference stripes), and may also exist in the auditory cortex and other structures [4,24–26]. In such structures, cells at various locations in the basic unit cell (e.g., a visual field) of the cortex (about 1 mm wide) respond preferentially to different stimulus features (e.g., eye, edge orientation, color, etc.). Cortical neurons are connected strongly to others with the same eye preference and visual field [4,24–26]. Outside their own visual field, they connect most strongly to cells with similar feature preference [4,24,26]. This leads to relatively nonspecific short-range connections, but patchy midrange ones. We thus seek a propagator that has an overall structure similar to the uniform-medium case, but which is modulated with the periodicity of the cortical structures.

We can generalize the role of $\hat{\nu}_{ab}$ in Eq. (7) to yield the form

$$P_{ab}(\mathbf{r},t) = \int d\mathbf{r}'\,dt'\,d\mathbf{r}''dt''\,\hat{\nu}_{ab}(\mathbf{r},\mathbf{r}'',t-t'') \times \Gamma_{ab}[\mathbf{r}''-\mathbf{r}',t''-t'-\tau_{ab}(\mathbf{r}''-\mathbf{r})]Q_b(\mathbf{r}',t'), \quad (17)$$

where we have also made the assumption that Γ_{ab} depends only on coordinate differences. The point $(\mathbf{r}'',t'')$ is the location at which axons b reach dendrites a, and the effective range in Γ_{ab} is just $r_{ab}=h_{ab}$ since the dendritic part is kept separate here (cf., Sec. II).

If we assume coupling operators of the form

$$\hat{\nu}_{ab}(\mathbf{r},\mathbf{r}'',t-t'') = \sum_{\zeta} \mathcal{S}_{\zeta ab}(\mathbf{r},t)\,\hat{\nu}_{\zeta ab}(\mathbf{r}-\mathbf{r}'',t-t''), \quad (18)$$

where the S_ζ are the strengths of the component operators $\hat{\nu}_\zeta$, which can have different spatial dependences, we can write

$$P_{ab}(\mathbf{r},t) = \sum_{\zeta} \mathcal{S}_{\zeta ab}(\mathbf{r},t)\,\psi_{\zeta ab}(\mathbf{r},t), \quad (19)$$

$$\psi_{\zeta ab}(\mathbf{r},t) = \int d\mathbf{r}''dt''\,\hat{\nu}_{\zeta ab}(\mathbf{r}-\mathbf{r}'',t-t'')\,\phi_{ab}(\mathbf{r}'',t''), \quad (20)$$

$$\phi_{ab}(\mathbf{r}'',t'') = \int d\mathbf{r}'\,dt'\,\Gamma_{ab}[\mathbf{r}''-\mathbf{r}',t''-t'-\tau_{ab}(\mathbf{r}''-\mathbf{r}')] \times Q_b(\mathbf{r}',t'). \quad (21)$$

When O is a differential operator, we can express the receptive field properties in differential form. In Fourier space, the convolution (20) has the form

$$\psi_{\zeta ab}(\mathbf{k},\omega) = \hat{\nu}_{\zeta ab}(\mathbf{k},\omega)\phi_{ab}(\mathbf{k},\omega). \tag{22}$$

With reference to the discussion in Sec. III, we now assume that the $\hat{\nu}_\zeta$ have the Fourier-space form [of which Eq. (14) is an example]

$$\hat{\nu}_\zeta(\mathbf{k},\omega) = \frac{R_\zeta(i\mathbf{k},-i\omega)}{W_\zeta(i\mathbf{k},-i\omega)}, \tag{23}$$

where R_ζ is a product of a power of $i\mathbf{k}$ and a power of $-i\omega$ and W_ζ is a polynomial (generally of a degree no lower than R_ζ) in these quantities, with unit constant term. In this case, we can write

$$W_{\zeta ab}(i\mathbf{k},-i\omega)\psi_{\zeta ab}(\mathbf{k},\omega) = R_{\zeta ab}(i\mathbf{k},-i\omega)\phi_{\zeta ab}(\mathbf{k},\omega), \tag{24}$$

and, hence

$$W_{\zeta ab}(\nabla,\partial_t)\psi_{\zeta ab}(\mathbf{r},t) = R_{\zeta ab}(\nabla,\partial_t)\phi_{\zeta ab}(\mathbf{r},t), \tag{25}$$

where $\partial_t = \partial/\partial t$. The differential equation (25) can be generalized by allowing slow variation of the coefficients of $W_{\zeta ab}$ with $\mathbf{r}$, a step that is not rigorously consistent with the foregoing analysis, but which is permissible given the approximate nature of our representation of the physiology, so long as d_a and t_a do not vary too rapidly on scales comparable to their own values. Alternatively, one could start with the generalized equation and derive more general versions of the preceding equations.

If one has a uniform-medium propagator $\Gamma^{(0)}_{ab}(\mathbf{r}-\mathbf{r}', t-t')$, and periodic spatial modulations are introduced that have the same form at all points and times, then Eq. (21) can be written as (with double primes omitted)

$$\phi_{ab}(\mathbf{r},t) = \sum_{\mathbf{K}} c_{ab\mathbf{K}}\phi_{ab\mathbf{K}}(\mathbf{r},t), \tag{26}$$

$$\phi_{ab\mathbf{K}}(\mathbf{r},t) = \int d\mathbf{r}'dt' e^{i\mathbf{K}\cdot(\mathbf{r}-\mathbf{r}')} \times \Gamma^{(0)}_{ab}[\mathbf{r}-\mathbf{r}', t-t'-\tau_{ab}(\mathbf{r}-\mathbf{r}')]Q_b(\mathbf{r}',t'), \tag{27}$$

where the $\mathbf{K}$ are the reciprocal lattice vectors of the periodic structure, and the $c_{ab\mathbf{K}}$ are the Fourier coefficients of the function that modulates the uniform-medium propagator. Note that reality of the fields implies $c_{ab\mathbf{k}} = c^*_{ab-\mathbf{K}}$.

We term the propagation implied by Eq. (27) *saltatory*. It is similar, but not identical, to the form for Bloch propagation in a periodic solid. The chief differences come about because (i) we use the propagator (11) of damped waves, rather than undamped ones, and (ii) our propagator is, perhaps paradoxically, translationally invariant (every point has patchy connections to its counterparts in other visual fields, and the structure of these connections is the same at all points), whereas the Bloch functions are tied to specific features of the crystal potential; the Bloch propagator can be treated as a superposition of saltatory propagators.

On Fourier transforming Eq. (27) we obtain

$$\phi_{ab\mathbf{K}}(\mathbf{k},\omega) = \Gamma^{(0)}_{ab}(\mathbf{k}-\mathbf{K},\omega)e^{i\omega\tau_{ab}}Q_b(\mathbf{k},\omega), \tag{28}$$

where we ignore spatial variations in τ_{ab} for simplicity (this restriction can be straightforwardly relaxed [28]). The component field $\phi_{ab\mathbf{K}}$ satisfies the dispersion relation

$$D^{(0)}_{ab}(\mathbf{k}-\mathbf{K},\omega)\phi_{ab\mathbf{K}}(\mathbf{k},\omega) = e^{i\omega\tau_{ab}}Q_b(\mathbf{k},\omega), \tag{29}$$

where $D^{(0)}_{ab}$ is the reciprocal of $\Gamma^{(0)}_{ab}$ in Fourier space. Fourier transforming Eq. (29) then yields

$$\left[\frac{1}{\gamma^2_{ab}}\frac{\partial^2}{\partial t^2} + \frac{2}{\gamma_{ab}}\frac{\partial}{\partial t} + 1 - r^2_{ab}(\nabla - i\mathbf{K})^2\right]\phi_{ab\mathbf{K}}(\mathbf{r},t) = Q_b(\mathbf{r},t-\tau_{ab}). \tag{30}$$

Using Eq. (28) and the Fourier transform of Eq. (26) we can thus write

$$\phi_{ab}(\mathbf{k},\omega) = e^{i\omega\tau_{ab}}\Gamma_{ab}(\mathbf{k},\omega)Q_b(\mathbf{k},\omega), \tag{31}$$

$$\Gamma_{ab}(\mathbf{k},\omega) = \sum_{\mathbf{K}} c_{ab\mathbf{K}}\Gamma^{(0)}_{ab}(\mathbf{k}-\mathbf{K},\omega). \tag{32}$$

If we write

$$\phi_{\mathbf{K}ab}(\mathbf{r},t) = e^{i\mathbf{K}\cdot\mathbf{r}}u_{ab\mathbf{K}}(\mathbf{r},t), \tag{33}$$

we find

$$\left[\frac{1}{\gamma^2_{ab}}\frac{\partial^2}{\partial t^2} + \frac{2}{\gamma_{ab}}\frac{\partial}{\partial t} + 1 - r^2_{ab}\nabla^2\right]u_{ab\mathbf{K}}(\mathbf{r},t) = e^{-i\mathbf{K}\cdot\mathbf{r}}Q_b(\mathbf{r},t-\tau_{ab}), \tag{34}$$

with the same operator on the left for all $\mathbf{K}$. By solving Eq. (34) for all values of $\mathbf{K}$ up to some upper bound, beyond which the component amplitudes are small enough to be neglected, we can obtain the $\phi_{ab\mathbf{K}}$ and, hence, ϕ_{ab}.

Equations (19), (24), (26), and (32) enable the evolution of $P_{ab}(\mathbf{r},t)$ to be followed in differential, rather than integral form, which is a great advantage numerically, especially as the coordinate-space propagators tend to have singularities [23]. If we Fourier transform these equations, assuming that $\mathcal{S}_\zeta$ is periodically varying in space and constant in time, such that

$$\mathcal{S}_{\zeta ab}(\mathbf{r},t) \approx \sum_{\mathbf{K}'} \mathcal{S}_{\zeta ab}(\mathbf{K}')e^{i\mathbf{K}'\cdot\mathbf{r}} \tag{35}$$

(the sum is replaced by an integral for a nonperiodic spatial variation), the above steps yield

$$P_{ab}(\mathbf{k},\omega) = \sum_{\zeta\mathbf{K}\mathbf{K}'} \mathcal{S}_{\zeta ab}(\mathbf{K}')\hat{\nu}_{\zeta ab}(\mathbf{k}-\mathbf{K}',\omega) \times c_{ab\mathbf{K}}\Gamma^{(0)}_{ab}(\mathbf{k}-\mathbf{K}'-\mathbf{K},\omega)e^{i\omega\tau_{ab}}Q_b(\mathbf{k}-\mathbf{K}',\omega) \tag{36}$$

$$= \sum_{\zeta\mathbf{K}'} \mathcal{S}_{\zeta ab}(\mathbf{K}')\hat{\nu}_{\zeta ab}(\mathbf{k}-\mathbf{K}',\omega) \times \Gamma_{ab}(\mathbf{k}-\mathbf{K}',\omega)e^{i\omega\tau_{ab}}Q_b(\mathbf{k}-\mathbf{K}',\omega). \tag{37}$$

If all the $\mathcal{S}_{\zeta ab}$ are the same for fixed a and b, the above analysis can be simplified by omitting the sum in Eq. (19),

dropping the subscript ζ, and treating R_ζ as a polynomial, rather than a monomial. All the suboperators are then combined into the single operator $\hat{\nu}$. Other simplifications include the case where only the $\mathbf{K}'=\mathbf{0}$ term is relevant, which corresponds to purely saltatory propagation, and the case where only $\mathbf{K}'=\mathbf{K}=\mathbf{0}$ is relevant, which corresponds to uniform-medium propagation.

V. LINEAR AND COUPLED-MODE PROPERTIES

Previous work has shown that a great variety of properties of brain electrical activity can be obtained by treating activity changes as being perturbations of a steady state [1,29]. We can study many properties of brain activity by solving the equations of Sec. II for a steady state and linearizing them relative to it. Here we allow for coupling of unperturbed modes via spatial variations of the model parameters and propagators (only the latter are discussed in detail here, while parameter variations in a restricted model have been discussed elsewhere [23,30]); fast temporal, possibly field-driven, parameter evolution can be included, but is not discussed here. We do *not* assume that the activity is uniform or constant.

A. Linear equations for activity

Of the relevant equations in Secs. II–IV, all but Eq. (5) are already linear in the fields. Equation (5) can be linearized by replacing the sigmoid S_a by its slope ρ_a at the assumed steady state value of V_a. If we assume for simplicity that ρ_a and L_{ab} are spatially constant, and Fourier transform the resulting set of linear equations in time, we find

$$Q_a(\mathbf{k},\omega)=\sum_{b\zeta\mathbf{K}'}\mathcal{S}_{\zeta ab}(\mathbf{K}')\hat{J}'_{\zeta ab}(\mathbf{k}-\mathbf{K}',\omega)\times\Gamma_{ab}(\mathbf{k}-\mathbf{K}',\omega)Q_b(\mathbf{k}-\mathbf{K}',\omega), \tag{38}$$

$$J^{\dagger}_{\zeta ab}(\mathbf{k}-\mathbf{K}',\omega)=\rho_a L_{ab}(\omega)\hat{\nu}_{\zeta ab}(\mathbf{k}-\mathbf{K}',\omega)e^{i\omega\tau_{ab}}. \tag{39}$$

Hence, if the $\hat{\nu}_{\zeta ab}$ are independent of wave number,

$$Q_a(\mathbf{k},\omega)=\sum_{b\mathbf{K}'}J^{\dagger}_{ab}(\mathbf{K}',\omega)\times\Gamma_{ab}(\mathbf{k}-\mathbf{K}',\omega)Q_b(\mathbf{k}-\mathbf{K}',\omega), \tag{40}$$

$$J^{\dagger}_{ab}(\mathbf{K}',\omega)=\sum_{\zeta}\rho_a L_{ab}(\omega)\mathcal{S}_{\zeta ab}(\mathbf{K}')\hat{\nu}_{\zeta ab}(\omega)e^{i\omega\tau_{ab}}, \tag{41}$$

which reproduces Eq. (27) of [2] in the present notation.

A useful alternative form of Eq. (38) is

$$\sum_{b\mathbf{K}'}\delta_{ab}\delta_{0\mathbf{K}'}Q_b(\mathbf{k}-\mathbf{K}',\omega)=\sum_{b\mathbf{K}'}X_{ab}(\mathbf{k},\mathbf{k}-\mathbf{K}',\omega)Q_b(\mathbf{k}-\mathbf{K}',\omega), \tag{42}$$

$$X_{ab}(\mathbf{k},\mathbf{k}-\mathbf{K}',\omega)=\hat{J}_{ab}(\mathbf{k},\mathbf{k}-\mathbf{K}',\omega)\Gamma_{ab}(\mathbf{k}-\mathbf{K}',\omega), \tag{43}$$

$$\hat{J}_{ab}(\mathbf{k},\mathbf{k}-\mathbf{K}',\omega)=\sum_{\zeta}\mathcal{S}_{\zeta ab}(\mathbf{K}')J^{\dagger}_{\zeta ab}(\mathbf{k}-\mathbf{K}',\omega), \tag{44}$$

where Eq. (44) defines $\hat{J}_{\zeta ab}(\mathbf{k},\mathbf{k}-\mathbf{K}',\omega)$.

An alternative form of Eq. (42) is obtained by setting $\mathbf{q}=\mathbf{k}-\mathbf{K}'$, which gives

$$\sum_{b\mathbf{q}}\delta_{ab}\delta_{\mathbf{k}q}Q_b(\mathbf{q},\omega)=\sum_{b\mathbf{q}}X_{ab}(\mathbf{k},\mathbf{q},\omega)Q_b(\mathbf{q},\omega), \tag{45}$$

which reproduces Eq. (30) of [2], in the present notation, if the $\hat{\nu}_{\zeta ab}$ are all wave number-independent, as was assumed in that previous work.

Successive simplifications to Eqs. (42)–(45) are possible in special cases: In the purely saltatory case, without parameter variations, only $\mathbf{K}'=\mathbf{0}$ need be considered, and the $\mathbf{k}$-modes are independent. If the propagators are nonpatchy, but their parameters vary spatially, then only $\mathbf{K}=\mathbf{0}$ is required. Finally, in the case of a nonpatchy, uniform-medium propagator, only $\mathbf{K}'=\mathbf{K}=\mathbf{0}$ need be included.

If there are N' neural populations in the system being considered, and J stimulus sources, and we assume that there is no direct feedback of stimuli on themselves, or of the brain on stimuli (as discussed further in [2]), then the matrix $\mathbf{X}$ is $(N'+J)\times(N'+J)$ in size, but the bottom J rows are zero. Hence Eq. (45) can be rewritten in the form

$$\sum_{b\mathbf{q}}A_{ab}(\mathbf{k},\mathbf{q},\omega)Q_b(\mathbf{q},\omega)=\sum_{j\mathbf{q}}B_{aj}(\mathbf{k},\mathbf{q},\omega)N_j(\mathbf{k},\omega), \tag{46}$$

$$A_{ab}(\mathbf{k},\mathbf{q},\omega)=\delta_{ab}\delta_{\mathbf{k}q}-X_{ab}(\mathbf{k},\mathbf{q},\omega), \tag{47}$$

and $B_{aj}(\mathbf{k},\mathbf{q},\omega)=X_{aj}(\mathbf{k},\mathbf{q},\omega)$, where b now denotes neural populations, j denotes external stimulus types, and N_j has been used in place of Q_j for the J stimulus types to emphasize the distinction between population firing rates and incoming stimulus pulse rates. The matrix $\mathbf{A}$ is $N'\times N'$ in size, while $\mathbf{B}$ has N' rows and J columns; the column matrix $\mathbf{N}$ has J elements, while the remaining column matrix $\mathbf{Q}$ now has N' elements. In the purely saltatory case ($\mathbf{K}'=0$) the modes are independent and Eqs. (45)–(47) become (upon dropping the redundant second arguments in A, B, X, and $\hat{J}$)

$$X_{ab}(\mathbf{k},\omega)=\hat{J}_{ab}(\mathbf{k},\omega)\Gamma_{ab}(\mathbf{k},\omega), \tag{48}$$

$$\sum_{b}A_{ab}(\mathbf{k},\omega)Q_b(\mathbf{k},\omega)=\sum_{j}B_{aj}(\mathbf{k},\omega)N_j(\mathbf{k},\omega), \tag{49}$$

$$A_{ab}(\mathbf{k},\omega)=\delta_{ab}-X_{ab}(\mathbf{k},\omega), \tag{50}$$

and likewise for B_{aj}. Equations (46)–(50) reproduce the corresponding results in [2] for nonpatchy Γ_{ab}.

It is useful to write Eq. (46) in matrix notation, by establishing a one-dimensional ordering of b and $\mathbf{K}$ to jointly label population and mode (see [2] for details). If Y is the product of the number of neural populations and the number of modes retained per population, and Z is the product of the number of stimulus channels and the number of modes per channel, this yields

$$\mathbf{Q} = \mathbf{TN}, \tag{51}$$

where the transfer matrix is $\mathbf{T}=\mathbf{A}^{-1}\mathbf{B}$, $\mathbf{A}$ is a $Y\times Y$ square matrix, $\mathbf{Q}$ is a $Y\times 1$ column matrix, $\mathbf{B}$ is a $Y\times Z$ rectangular matrix, and $\mathbf{N}$ is a $Z\times 1$ column matrix.

B. Linear waves, observables, spectra, and correlations

The dispersion relation of linear waves in the system is given by

$$\det \mathbf{A}(\mathbf{k},\omega) = 0, \tag{52}$$

and the system is stable at $\mathbf{k}$ if all the frequency roots of this equation have negative imaginary parts. If the steady state is stable for all $\mathbf{k}$, spectra, correlations, and other properties of the linear perturbations can be self-consistently defined.

A measurable scalar quantity ψ may be able to be approximated by a linear combination of the Q_a (e.g., a scalp potential may involve contributions from several cellular populations, with various weights). In this case, at a given $\mathbf{k}$ and ω,

$$\psi = \mathbf{MQ} = \mathbf{MTN}, \tag{53}$$

where $\mathbf{M}$ is a row vector of complex measurement coefficients. The power spectrum of ψ is

$$P(\mathbf{k},\omega) = |\psi(\mathbf{k},\omega)|^2. \tag{54}$$

VI. GAMMA OSCILLATIONS

This section is devoted to understanding the role of patchy connections in supporting gamma oscillations in the corticothalamic system. We first state the key results needed from the model of corticothalamic dynamics developed in previous papers (e.g., [2] and references cited therein). We then generalize the propagators to the saltatory case to illustrate the main effects of nonuniform propagation, without having to incorporate the full complexities of Bloch propagators. Relevant approximations to enable analytic insights are then made, and the spatiotemporal spectral properties of the improved model are investigated. In order to focus on the key physics, we ignore the effects of volume conduction, which would need to be included to consider signals recorded at the scalp, but which is not relevant to most studies of gamma oscillations, which are carried out at the cortex itself.

A. EMIRS corticothalamic model

In previous studies we introduced a model of the cortex and thalamus, including separate long-range excitatory (subscript e), midrange excitatory (m), and short-range inhibitory (i) populations in the cortex, plus the reticular (r) and specific (or relay; s) thalamic nuclei. The $\hat{\nu}$ were assumed to be spatially uniform and k-independent, and only one value of ζ was considered. We termed this the EMIRS model, and Fig. 1 shows its connectivities. Within the cortex, random connectivity was assumed, implying that all the gains G_{cb} are equal for fixed b, with c denoting a cortical population. We also assumed a common sigmoidal function and used the parameters in Table I to justify a number of simplifications. In Sec. VI C we illustrate the differences involved in introducing more general propagators via their effects on the linear EEG spectrum. We stress that the parameters in Table I are all consistent with independent experimental measurements, as explained in detail in Ref. [1], and are not free parameters. The effects found below are thus a consequence of the parameters, not vice versa.

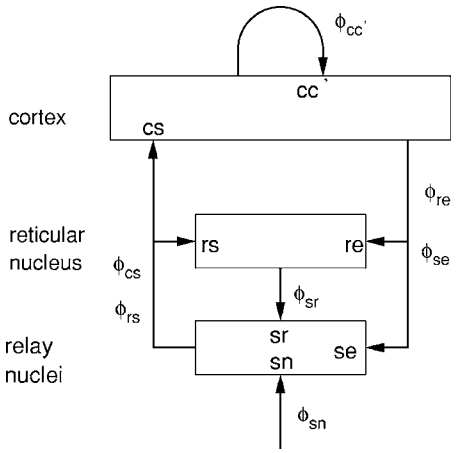

FIG. 1. Schematic of the connectivities in the EMIRS corticothalamic system. The cortical populations $(c,c'=e,m,i)$, reticular nucleus (r), and specific relay nuclei (s) are shown. Also shown are the pulse-rate fields ϕ_{ab} that propagate from population b to population a, including external inputs ϕ_{sn}.

We previously found the linear transfer function for ϕ_{ee}/ϕ_{sn} [2]. Here, we are interested in Q_e/Q_n, which relates more directly to the main class of intracellular measurements of gamma oscillations. This is obtained from the analysis in Sec. V by calculating the matrices $\mathbf{A}$, $\mathbf{B}$, and $\mathbf{T}=\mathbf{A}^{-1}\mathbf{B}$, then selecting the element that relates Q_e to $Q_n(\approx\phi_{sn})$, giving

$$\frac{Q_e(\mathbf{k},\omega)}{Q_n(\mathbf{k},\omega)} = X_{es}X_{sn}[(1-X_{sr}X_{rs})(1-X_{ee}-X_{em}-X_{ei}) - X_{es}(X_{se}+X_{sr}X_{re})]^{-1}, \tag{55}$$

where

$$X_{ab} = X_{ab}(\mathbf{k},\omega) = \hat{J}_{ab}(\mathbf{k},\omega)\Gamma_{ab}(\mathbf{k},\omega) \tag{56}$$

[cf., Eq. (48)]. This general form is unchanged if saltatory propagators are used in place of the uniform-medium ones of our previous work, if the $\hat{\nu}$ are allowed to be $\mathbf{k}$-dependent but spatially uniform differential operators, and/or if more than one value of ζ is permitted (although we consider only a single value here). The corresponding transfer function ϕ_{ee}/ϕ_{sn} is the same except that it has an extra denominator $k^2r_{ee}^2+q_{0ee}^2r_{ee}^2$ for the relevant parameters.

We previously estimated the parameters in this model, apart from measures of nonuniformity; these previous estimates are summarized in Table I. Here we note that the midrange m connections are known to be patchy, with strong modulation, while patchy or localized inputs to visual cortex, from the lateral geniculate nucleus of the thalamus, arise from stimuli that are localized and have edges with a particu-

TABLE I. Brain parameters for normal adults in the alert, eyes-open state from [2], apart from the basic lattice vector, which presumes a spatial periodicity of 1 mm. The first column gives a brief description of the parameter, with its symbol listed in the second. The third column gives the estimates of the new parameters used previously, while the unit of each quantity is given in the final column. Only nonzero values for connections that are retained here are listed. All the r_{ab} and v_{ab} values are estimated for the visual system and are given in terms of dimensional map coordinate units and must be multiplied by the scale of the target structure relative to the cortex (0.1 for the human thalamus, as discussed in [2] to obtain actual physical values. All the synaptodendritic rates have been assumed equal, regardless of a and b, and the index c denotes cortical populations e,m,i. The gains G_{ab} that correspond to the $\mathbf{K}=\mathbf{0}$ resonance are defined by Eq. (61). The reason for sum $G_{cm}+G_{ci}$ appearing in the second column is that only the sum of these two quantities has been determined with reasonable accuracy in previous human studies; in the present work we assume $G_{cm}=6.9(\approx G_{ce})$ and $G_{ci}=-15.0$.

Quantity	Symbol	Estimate	Unit
Propagation delays	τ_{re},τ_{se}	43	ms
	τ_{cs}	43	ms
Synaptodendritic rates	α_{ab}	80	s^{-1}
	β_{ab}	800	s^{-1}
Gains	G_{ce}	6.8	
	$G_{cm}+G_{ci}$	−8.1	
	G_{cs}	1.7	
	G_{re}	1.0	
	G_{rs}	0.19	
	G_{se}	2.5	
	G_{sr}	−1.9	
	G_{sn}	0.8	
Projection ranges	r_{ce}	85	mm
	r_{cm}	2	mm
	r_{ci}	0.2	mm
	r_{re},r_{se}	1.2	mm
	r_{cs}	0.3	mm
	r_{rs}	1.2	mm
	r_{sr}	1.2	mm
	r_{sn}	1.2	mm
Projection velocities	v_{ce}	10	m s^{-1}
	v_{cm}	1	m s^{-1}
	v_{ci}	0.3	m s^{-1}
	v_{re},v_{se}	36	m s^{-1}
	v_{cs}	3.6	m s^{-1}
	v_{rs}	2	m s^{-1}
	v_{sr}	2	m s^{-1}
	v_{sn}	70	m s^{-1}
Damping rates	γ_{ce}	120	s^{-1}
	γ_{cm}	500	s^{-1}
	γ_{ci}	1500	s^{-1}
	γ_{re},γ_{se}	3×10^4	s^{-1}
	γ_{cs}	1.2×10^4	s^{-1}
	γ_{rs}	1700	s^{-1}
	γ_{sr}	1700	s^{-1}
	γ_{sn}	6×10^5	s^{-1}
Lowest lattice vector	K	6000	m^{-1}

lar orientation [4,10,20,24–26]. This latter effect arises from the fact that each visual receptive field corresponds to one cortical *hypercolumn* of circa 1 mm in linear extent, and each orientation is sensed at a specific location within that hypercolumn [4,24–26]. Grating stimuli, for example, are thus able to excite very localized cortical areas in the first instance (although the resulting activity then propagates to neighboring regions). Here, we consider only white-noise stimulation via either smooth or patchy *es* propagators, with $\hat{G}$ the same for all locations. This saltatory approximation enables us to examine the main physical effects of patchy propagation without resorting to the full Bloch formalism; the latter can be expected to exhibit even stronger effects resulting from nonuniformities.

B. Gamma resonances

We next determine the nature of gamma resonances in the transfer function (54). For analytic purposes below (but not in the numerical calculations), we note that gamma oscillations occur at frequencies well above the characteristic resonant frequency $\omega\approx 2\pi/t_0$ of corticothalamic loops, where there are also additional steps of low-pass filtering relative to purely corticocortical couplings. Hence corticothalamic feedback can be neglected to a good approximation (which we have verified numerically for the parameters in Table I) when studying gamma oscillations, and thalamic signals Q_s can be treated as the input stimuli to an otherwise isolated cortex. This yields the transfer function

$$\frac{Q_e(\mathbf{k},\omega)}{Q_s(\mathbf{k},\omega)}=\frac{X_{es}}{1-X_{ee}-X_{em}-X_{ei}}. \tag{57}$$

The key high-frequency resonances in Eq. (57) arise from zeros of the denominator; i.e., where

$$1-X_{ee}-X_{em}-X_{ei}=0. \tag{58}$$

In the short-scale, high-frequency case, the term X_{ee} can be neglected. Moreover, as each of the other terms in Eq. (57) usually proves to dominate at a distinct location in ω-$\mathbf{k}$ space, Eq. (58) can sometimes be simplified to $X_{eb}=1$, with $b=m$ or $b=i$.

The condition $X_{em}+X_{ei}=1$ yields

$$\sum_{\mathbf{K}}\frac{\hat{G}(\mathbf{k},\omega)}{(\mathbf{k}-\mathbf{K})^2r_{em}^2+(1-i\omega/\gamma_{em})^2}=\left(1-\frac{i\omega}{\alpha_{em}}\right)\left(1-\frac{i\omega}{\beta_{em}}\right)-\frac{G_{ei}}{k^2r_{ei}^2+1}, \tag{59}$$

with

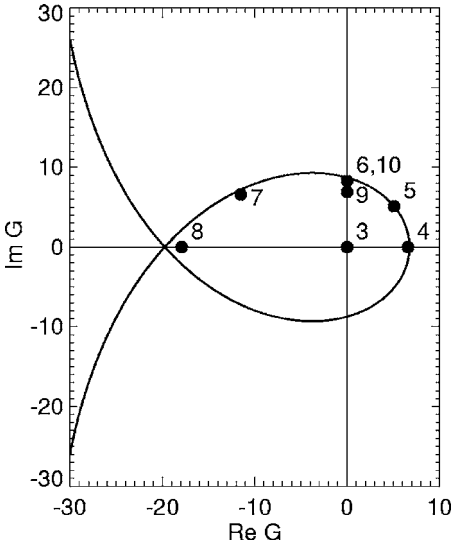

FIG. 2. Instability locus from Eq. (62) in the complex $\hat{G}$ plane with parameters from Table I, $G_{em}=6.9$, and $G_{ei}=-15$. Stable values of $\hat{G}$ lie within the inner loop. The approximate values of $\hat{G}$ corresponding to Figs. 3–10 are numbered accordingly. Note that the graphics package used does not permit carets to be inserted above the G's labeling the axes.

$$\hat{G}(\mathbf{k},\omega)=\rho_e\hat{\nu}_{em}(\mathbf{k},\omega)c_{em\mathbf{K}}, \tag{60}$$

$$G_{ab}=\rho_a\hat{\nu}_{ab}(\mathbf{0},\omega), \tag{61}$$

where the only nonzero ei term is the one shown, and we have assumed $\omega\ll\gamma_{ei}$. If the denominator corresponding to $\mathbf{K}$ is very small on the left side of Eq. (59), this term dominates the sum. If $\hat{G}$ represents a purely spatial receptive field, its argument ω can be omitted and Eq. (59) becomes

$$\hat{G}=\left[\left(1-\frac{i\omega}{\alpha_{em}}\right)\left(1-\frac{i\omega}{\beta_{em}}\right)-\tilde{G}_{ei}\right]\times\left[(\mathbf{k}-\mathbf{K})^2r_{em}^2+\left(1-\frac{i\omega}{\gamma_{em}}\right)^2\right], \tag{62}$$

where $\hat{G}=\hat{G}(\mathbf{K})$ and $\tilde{G}_{ei}=G_{ei}/(K^2r_{ei}^2+1)$. Note that, generally, one must retain the $\pm\mathbf{k}$ and $\pm\mathbf{K}$ terms to ensure that the fields are real, but only one term at a time need be retained to study stability. Ultimately, the magnitude of $\hat{G}(\mathbf{K})$ will decrease for large values of K, so the dominant instabilities will tend to be due to the lowest terms.

Equation (62) is a quartic in ω that can be solved explicitly, but the general solutions are not very informative, owing to their complexity. Some insights into the solutions can be obtained in useful special cases, which we address next.

At marginal stability (i.e., exact resonance), with $G_{ei}=0$, the frequency is real and the real and imaginary parts of Eq. (62) become

$$\left(1-\frac{\omega^2}{\alpha\beta}\right)\left(p^2+1-\frac{\omega^2}{\gamma^2}\right)-\frac{2\omega^2(\alpha+\beta)}{\alpha\beta\gamma}=\mathrm{Re}\,\hat{G}, \tag{63}$$

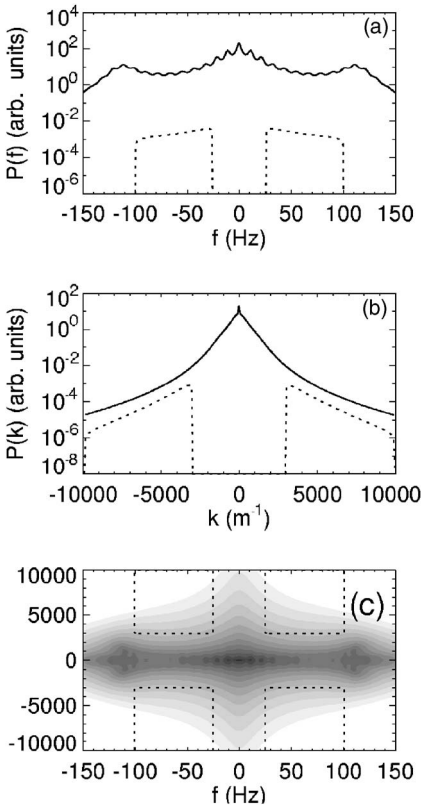

FIG. 3. Spectra for parameters in Table I and $\hat{G}=0$. (a) Unfiltered (solid) and filtered (dotted) $P(f)$. (b) Unfiltered and filtered $P(k)$. (c) $P(f,k)$ with grayscale increasing in half-decade steps from a minimum of 10^{-9}; dashed lines bound the filter passbands.

$$\omega\left[\frac{\alpha+\beta}{\alpha\beta}\left(p^2+1-\frac{\omega^2}{\gamma^2}\right)+\frac{2}{\gamma}\left(1-\frac{\omega^2}{\alpha\beta}\right)\right]=\mathrm{Im}\,\hat{G}, \tag{64}$$

respectively, with $p^2=|\mathbf{k}-\mathbf{K}|^2$, where we omit the subscripts em on α, β, and γ in Eqs. (63) and (64). Sharp resonances will be found close to the point where these equations are satisfied.

If $\mathrm{Im}\,G=0$ one solution of Eq. (64) is at $\omega=0$, which is not relevant to gamma oscillations. The other solution is

$$\omega^2=\frac{\gamma[2\alpha\beta+\gamma(\alpha+\beta)(1+p^2)]}{\alpha+\beta+2\gamma}, \tag{65}$$

which increases monotonically when α, β, γ, or p increases. In this case, instability occurs at a critical value of $\hat{G}$ given by [2]

$$\hat{G}=-\frac{2(\alpha'+\beta')(1+\alpha')^2(1+\beta')^2}{\alpha'\beta'(\alpha'+\beta'+2)^2}, \tag{66}$$

where $\alpha'=\alpha/\gamma$ and $\beta'=\beta/\gamma$.

If $G_{ei}=0$ the approximate solutions to Eq. (62) and its counterpart with $\mathbf{k}\approx-\mathbf{K}$ are

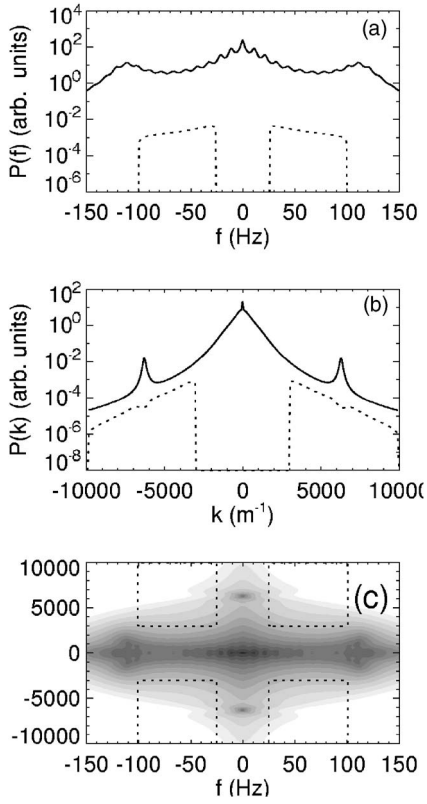

FIG. 4. Spectra, as in Fig. 3 except for $\hat{G}=6.6$. (a) $P(f)$. (b) $P(k)$. (c) $P(f,k)$.

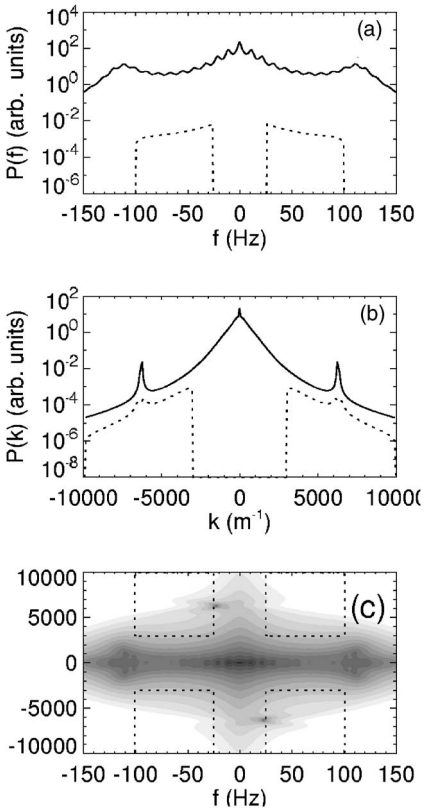

FIG. 5. Spectra, as in Fig. 3 except for $\hat{G}=5.1+5.1i$. (a) $P(f)$. (b) $P(k)$. (c) $P(f,k)$.

$$\omega = \pm \frac{\arg \hat{G}}{\frac{1}{\alpha}+\frac{1}{\beta}+\frac{2}{\gamma}}, \tag{67}$$

for $|\omega| \lesssim \alpha \ll \beta, \gamma$. Equation (67) is modified at larger ω, but the trend for ω to increase approximately linearly with $\arg \hat{G}(\leqslant \pi)$ continues.

Figure 2 shows the locus of the right side of Eq. (62) for the parameters in Table I, with $G_{em}=6.9$ and $G_{ei}=-15$. We see that, no matter what the value of $\arg \hat{G}$, the instability locus is reached for finite $|\hat{G}|$. If $|G_{ei}|$ is reduced toward zero, the locus generally moves inward, with intercepts for $G_{ei}=0$ of $+1$ on the positive real axis, and a value given by Eq. (66) on the negative real axis.

C. Spectra

Previous work has shown that assumption of approximately white noise inputs to the corticothalamic system gives good agreement with a wide range of experimental data on EEG-related phenomena, including spectra [1,3,23,28–33], which are predominantly generated by long-range excitatory neurons in the cortex, except on the finest spatial scales where the other cortical populations contribute [28,30,33]. The validity of the white noise approximation is additionally supported by the Poissonian nature of neural spikes, and by the fine-scale spatial granularity of synapses, in real neural systems. Here we explore the spectral properties of our system on the assumption of white noise inputs to probe the effects of the patchy propagators. The qualitative effects of nonwhite inputs are then considered briefly.

Many experiments on gamma oscillations bandpass filter the observed spike-rate and EEG-related signals in frequency. They also often use short (a few mm) arrays of electrodes for measurements, which correspond to bandpass spatial filtering between a lower wave-number bound $k \approx 2\pi/L$ imposed by the array length L (a few mm), and an upper bound $k=2\pi/l$ imposed by the electrode size l (a fraction of a mm). In this section we discuss both unfiltered and bandpass-filtered spectra. For illustrative purposes, the frequency filter here passes frequencies between 25 and 100 Hz, and wave numbers between 3000 and 2×10^4 m^{-1}, with roll-offs of approximately 10% of the pass range at each end.

Figure 3(a) shows the frequency spectrum $P_{ee}(f)$, with $f=\omega/2\pi$, for the uniform-medium parameters in Table I, and $\hat{G}=6.9$, corresponding to location 3 in Fig. 2. As in previous work, the frequency spectrum shows the alpha and beta peaks, and higher harmonics, which are due to corticothalamic resonances at circa 10 and 20 Hz, etc., respectively, in this theory [29,32]. There is a steepening at $f \gtrsim 20$ Hz, caused by the onset of synaptodendritic low-pass filtering [23,29,32], but this is interrupted by a broad, low-k enhancement near 110 Hz caused by the ei gamma resonance found in recent work [2] and obtainable from Eq. (59) by omitting the em quantities. The filtered spectrum is featureless because the thalamic feedbacks are strongest at low k and are

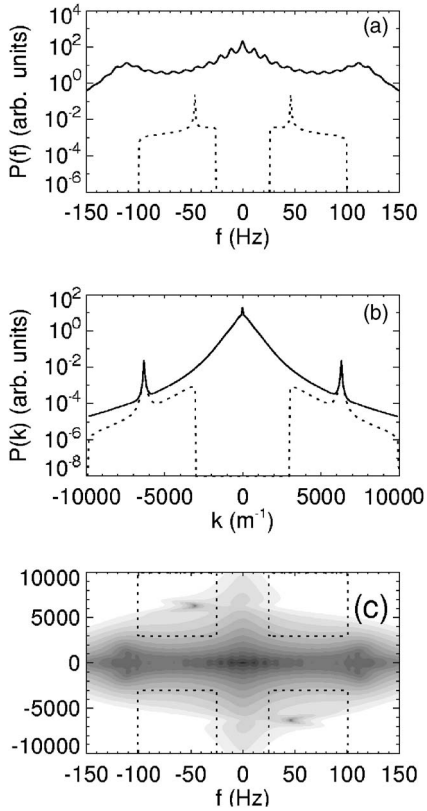

FIG. 6. Spectra, as in Fig. 3 except for $\hat{G}=8.3i$. (a) $P(f)$. (b) $P(k)$. (c) $P(f,k)$.

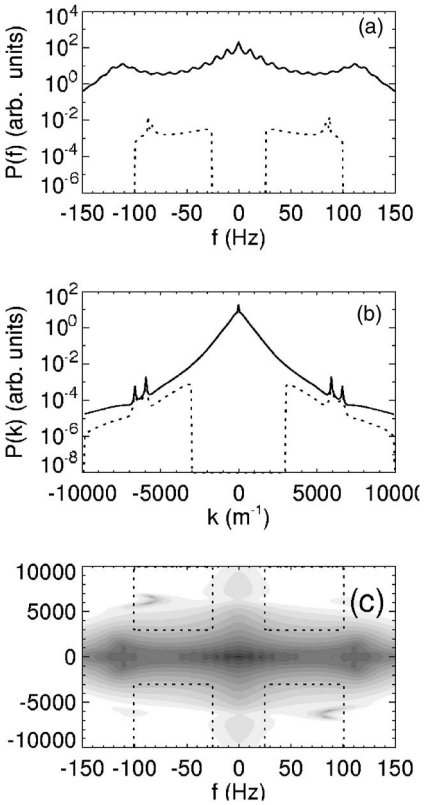

FIG. 7. Spectra, as in Fig. 3 except for $\hat{G}=i-11.5+6.6i$. (a) $P(f)$. (b) $P(k)$. (c) $P(f,k)$.

thus removed by the filter. The corresponding wave-number spectrum in Fig. 3(b) falls off at $k \gtrsim 1/r_{ee} \approx 10$ m^{-1} [28,30]. These aspects encapsulate key features of the combined frequency-wave-number spectrum $P_{ee}(k,\omega)$ shown in Fig. 3(c). Again, the filtered spectrum is featureless.

Figure 4 shows the same case as Fig. 3, except with $\hat{G}_{em}=6.6$, corresponding to the location shown in Fig. 2. The chief differences from Fig. 3 are that the combined spectrum has new peaks at $f=0$, $k=\pm K$ (where K is the smallest lattice vector, henceforth), arising from the *em* resonance in Eq. (59), and coinciding with a pair of roots of the quartic equation (62). The propagator structure thus induces neural activity structure on the scale of the propagator periodicity. The frequency and wave-number spectra show corresponding enhancements, although these are absent in the filtered spectra because of their bandpass characteristics.

Figures 5–8 are the same as Fig. 4, but with $\arg \hat{G}$ increasing, as shown in Fig. 2, while $\hat{G}$ remains near the instability boundary. The two high-k peaks in the combined spectra [panels (c)] are shifted to frequencies that follow the general increasing trend discussed in connection with Eq. (67) (where G_{ei} was neglected), thus yielding gamma oscillations with short wavelengths, as inferred from experiments [4–19] that show fine-scale structure in gamma properties, especially during perception. The most intense waves follow approximately parabolic loci, corresponding to the evenness in $k-K$ implicit in Eq. (62), each following a root of Eq. (62) or its analog for $\mathbf{k}=-\mathbf{K}$ [symmetry between ω, $\mathbf{k}$ and $-\omega$, $-\mathbf{K}$

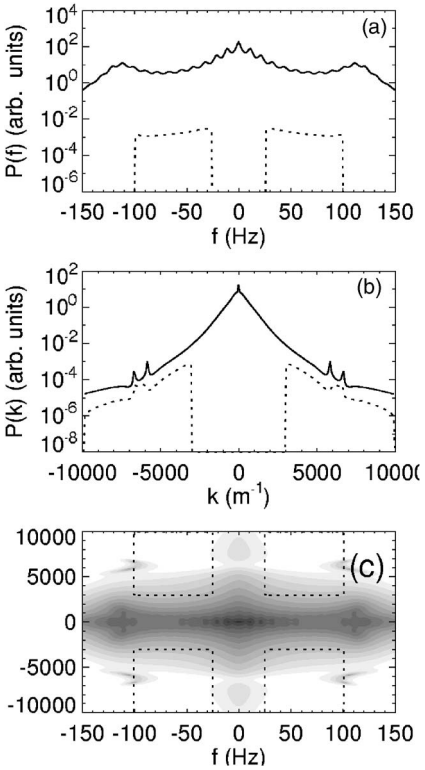

FIG. 8. Spectra, as in Fig. 3 except for $\hat{G}=-17.9$. (a) $P(f)$. (b) $P(k)$. (c) $P(f,k)$.

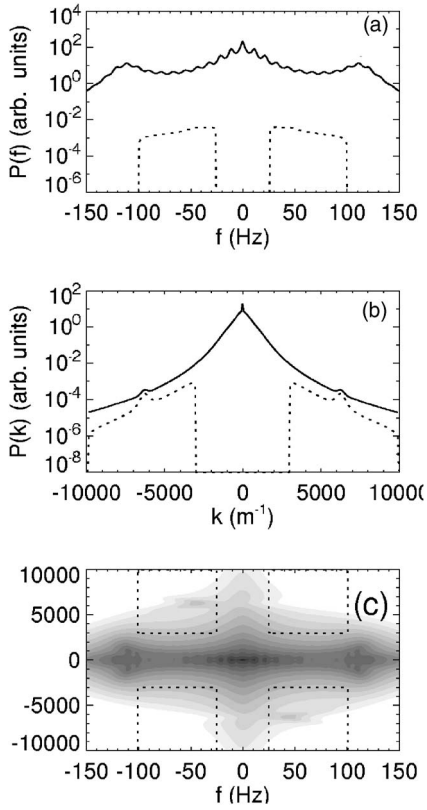

FIG. 9. Spectra, as in Fig. 6 except for $\hat{G}=6.9i$. (a) $P(f)$. (b) $P(k)$. (c) $P(f,k)$.

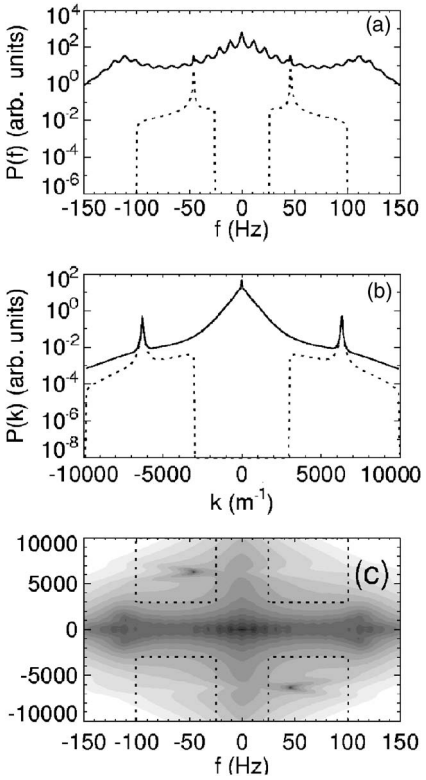

FIG. 10. Spectra, as in Fig. 6 except for $\hat{G}_{cs\mathbf{K}}=G_{cs}=1.7$. (a) $P(f)$. (b) $P(k)$. (c) $P(f,k)$.

is a consequence of the reality of $Q_e(\mathbf{r},t)$]. The filtered spectra show strong peaks in k and (when the peak is within the frequency passband) f; the latter of which is not seen in the unfiltered frequency spectrum. This last feature, plus the high-k attenuation caused by volume conduction in the skull, explains why gamma enhancements are very noticeable in intracranial experiments, but relatively weak at large scales, such as those of EEG experiments.

Figures 5–8 are in accord with experimental observations that gamma frequencies can be highly variable, but that the bandwidths are small in individual measurements [9,11,13,16]. This feature permits relatively large correlation lengths and times, and thus explains widespread experimental observations that long-range (several mm or more) synchronization is closely associated with the occurrence of oscillatory activity and local field potentials [5,12,15,17,18].

The cases explored in Figs. 4–8 are located near the instability boundary, as seen from Fig. 2. Figure 9 shows the effect of reducing the magnitude of $\hat{G}$ by about 15% relative to the case seen in Fig. 6 but keeping $\arg \hat{G}$ constant: the high-k peaks are greatly weakened. Hence we conclude that gamma resonances will be prominent only for systems with relatively low stability. This is consistent with numerous qualitative arguments in the neuroscience literature to the effect that the brain must be only weakly stable if it is to exhibit complex behavior, and with our own quantitative measures of this weak stability [23,32].

In order to examine the effects of spatially structured inputs to the cortex, which may arise from stimulus correlations or structure in thalamocortical connections, Fig. 10 is plotted for the same case as Fig. 6, but with patchy *es* connections satisfying $\hat{G}_{es\mathbf{K}}=G_{es}$. As might be expected, it shows enhanced high-k and high-f activity, resulting from the additional fine-scale structure imposed.

VII. SUMMARY AND DISCUSSION

Propagator theory of brain dynamics [2] has been extended to treat periodically modulated propagation by introducing Bloch-like patchy propagators of localized waves; a special case of saltatory propagators has also been recognized, in which the propagators are periodically modulated, but their form is translationally invariant. Improved integral and differential representations of receptive-field operators were also derived in forms suitable for use in mean-field theories. Linear properties of waves obeying patchy propagators were then derived.

The results were applied to explore the effects of including saltatory propagation in the widely successful EMIRS corticothalamic model to determine whether they can account for the spatiotemporal characteristics of EEG waves in the gamma frequency range. It was found that each reciprocal lattice vector can lead to a resonance in the transfer function and, hence, that dispersion and stability properties at high wave number are dominated by these resonances. This enabled approximate expressions for resonance frequencies and stability to be developed.

Numerical calculation of spectra resulting from driving the EMIRS model with white noise showed that the inclusion

of spatial structure in the propagators results in resonances at the lattice wave number, with frequencies between 0 and roughly 100 Hz for physiologically realistic parameters taken from previous studies. These resonances were narrow band, but their frequency can vary over a wide range, depending on the receptive field properties—both properties are in agreement with experiments, but the possible connection of frequency to receptive properties does not appear to have been previously discussed experimentally, except in connection with stimulus velocity [11]. In that case, temporally dependent receptive fields (not considered in detail here) would likely produce similar changes in $\arg \hat{G}$ to those induced by spatial stimulus gradients, leading to the observed frequency shifts via analogous mechanisms to those found here.

Numerical results imply that resonances in the gamma range ($\gtrsim$30 Hz) require parameters that bring the system close to high-k instability, and which generally involve complex-valued receptive field couplings in Fourier space. For frequencies to lie in the gamma range for the parameters in Table I (or for similar values of α_{ab}, β_{ab}, and γ_{ab}), $\arg \hat{G} \gtrsim \pi/2$ is required. This implies that the coupling is not purely related to the intensity of the stimulus (in which case it would be real), but involves spatiotemporal gradients of the stimulus field—a known feature of actual receptive fields in the visual cortex, for example. It also implies that analogous, lower-frequency perception-related oscillations may be relevant in cases where stimulus intensity is the primary feature of relevance, for example. Coherent beta (approximately 13–30 Hz) oscillations have been found in monkeys performing combined visual discrimination and motor tasks [34].

The finding that significant resonances are only present when the system is close to the relevant instability boundary accord with our previous results that showed that the brain operates close to marginal stability, thereby permitting a wide range of complex behavior. Moreover, the sharp fall off of resonant activity with distance from the boundary enables incoming stimuli to adjust the amount of resonant activity easily without changing the mean activity level by much (gains are approximately proportional to activity [1,23]), consistent with gamma oscillations being due to "stimulus evoked resonances" [11].

The above points are consistent with the resonances identified here being responsible for observed gamma enhancements during experiments on visual perception, as discussed in the references cited above. In such experiments, intracellularly observed gamma oscillations often display fine structure down to scales of a few tenths of a mm. Thus it appears that the introduction of observed spatial variations in propagators, of the qualitative scale and types that are known to occur, is sufficient to account for the key frequency-wavenumber characteristics of gamma oscillations. Further quantitative comparisons of correlation and coherence properties, and a more detailed representation of the spatial variation of receptive-field properties using Bloch functions, will establish this correspondence in detail.

ACKNOWLEDGMENT

The Australian Research Council supported this work.

[1] P. A. Robinson, C. J. Rennie, D. L. Rowe, and S. C. O'Connor, Hum. Brain Mapp **23**, 53 (2004).
[2] P. A. Robinson, Phys. Rev. E **72**, 011904 (2005).
[3] D. L. Rowe, P. A. Robinson, and C. J. Rennie, J. Theor. Biol. **231**, 413 (2004).
[4] C. Koch, *Biophysics of Computation* (Oxford, Oxford, 1999).
[5] P. König and A. K. Engel, Curr. Opin. Neurobiol. **5**, 511 (1995).
[6] A. K. Engel, P. König, A. K. Kreiter, T. B. Schillen, and W. Singer, Trends Neurosci. **15**, 218 (1992).
[7] P. R. Roelfsema, A. K. Engel, P. König, and W. Singer, Nature (London) **385**, 157 (1997).
[8] A. K. Engel, P. König, A. K. Kreiter, and W. Singer, Science **252**, 1177 (1991).
[9] A. K. Engel, P. König, C. M. Gray, and W. Singer, Eur. J. Neurosci. **2**, 588 (1990).
[10] D. Y. T'so, C. D. Gilbert, and T. N. Wiesel, J. Neurosci. **6**, 1160 (1986).
[11] R. Eckhorn, R. Bauer, W. Jordan, M. Brosch, W. Kruse, M. Munk, and H. J. Reitboeck, Biol. Cybern. **60**, 121 (1988).
[12] P. König, A. K. Engel, and W. Singer, Proc. Natl. Acad. Sci. U.S.A. **92**, 290 (1995).
[13] C. M. Gray, P. König, A. K. Engel, and W. Singer, Nature (London) **338**, 334 (1989).
[14] P. Fries, P. R. Roelfsema, A. K. Engel, P. König, and W. Singer, Proc. Natl. Acad. Sci. U.S.A. **94**, 12699 (1997).
[15] A. K. Engel and W. Singer, Trends Neurosci. **5**, 16 (2001).
[16] W. Singer, Annu. Rev. Physiol. **55**, 349 (1993).
[17] W. Singer and C. M. Gray, Annu. Rev. Neurosci. **18**, 555 (1995).
[18] P. E. Maldonado, S. Friedman-Hill, and C. M. Gray, Cereb. Cortex **10**, 1117 (2000).
[19] A. K. Engel, P. R. Roelfsema, P. Fries, M. Brecht, and W. Singer, Cereb. Cortex **7**, 571 (1997).
[20] W. H. Bosking, Y. Zhang, B. Schofield, and D. Fitzpatrick, J. Neurosci. **17**, 2112 (1997).
[21] P. C. Bressloff, Phys. Rev. Lett. **89**, 088101 (2002).
[22] P. C. Bressloff and J. D. Cowan, Phys. Rev. Lett. **88**, 078102 (2002).
[23] P. A. Robinson, C. J. Rennie, and J. J. Wright, Phys. Rev. E **56**, 826 (1997).
[24] *Principles of Neural Science*, 3rd ed., edited by E. R. Kandel, J. H. Schwartz, and T. M. Jessell (Appleton and Lange, Norwalk, 1991).
[25] P. Dayan and L. F. Abbott, *Theoretical Neuroscience* (MIT, Cambridge, 2001).
[26] R. L. De Valois and K. K. De Valois, *Spatial Vision* (Oxford University Press, Oxford, 1990).
[27] *Handbook of Mathematical Functions*, edited by M. Abramowitz and I. A. Stegun (Dover, New York, 1970).

[28] S. C. O'Connor and P. A. Robinson, Phys. Rev. E **67**, 051912 (2003).
[29] P. A. Robinson, C. J. Rennie, and D. L. Rowe, Phys. Rev. E **65**, 041924 (2002).
[30] S. C. O'Connor, P. A. Robinson, and A. K. I. Chiang, Phys. Rev. E **66**, 061905 (2002).
[31] C. J. Rennie, J. J. Wright, and P. A. Robinson, J. Theor. Biol. **205**, 17 (2000).
[32] P. A. Robinson, C. J. Rennie, J. J. Wright, H. Bahramali, E. Gordon, and D. L. Rowe, Phys. Rev. E **63**, 021903 (2001).
[33] C. J. Rennie, P. A. Robinson, and J. J. Wright, Biol. Cybern. **86**, 457 (2002).
[34] A. Brovelli, M. Z. Ding, A. Ledberg, Y. H. Chen, R. Nakamura, and S. L. Bressler, Proc. Natl. Acad. Sci. U.S.A. **101**, 9849 (2004).